GOLD-POLYMER HYBRID METASURFACE FOR POLARIZATION INDEPENDENT ENHANCED THIRD HARMONIC GENERATION IN THE ULTRAVIOLET : SUPPLEMENTAL DOCUMENT

Simulation method FDTD:

The Finite Difference Time Domain (**FDTD)** method from Lumerical software was used to analyse the electric field confinement and enhancement obtained in the quasi-3D photonics crystals. The FDTD method is the process of translating Maxwell's Equation into a form of approximation electromagnetic fields of any complex geometric structures and devices by confining the source in one small area of the surface.[41-43] This type of computational technique is very suitable for our proposed structure as it provides us with both the spatial and temporal properties of the structure with a single calculation thus making it suitable for the analysis of a various range of parameters. In the simulation setup, a one-cell area of the hexagonal lattice was set as a domain. Periodic boundary conditions are imposed in x and y axes and perfectly matched layers (PML) are imposed in z axes. For more accurate spatial computation, a conformal mesh of 1 nm steps is defined around the metal-dielectric boundaries.

The E field injection for linear characterization was a plane-wave light source in the x-y plane, having a broadband spectrum ranging from 400 nm to 1200 nm (near-infrared), to match the range of the supercontinuum laser used to characterize the samples in the laboratory experiments.

1. The frequency domain field monitors in the FDTD solvers record the electric and magnetic fields at a series of user-defined frequencies. R and T are representations of Far field reflectivity(R) and Transmission(T), respectively. We choose the CW (Continuous Wave) normalization throughout all sets of computations to make sure the results are easier to interpret. CW normalization gives the detected R/T = $\left|\frac{E_z(\omega)}{S(\omega)}\right|^2$, where S(w) is the spectrum of the source and $E_z(\omega)$ is the spectrum of the far field detected signal.
2. E field map is given by the computed variations in the electric field amplitude spatially detected across a planar surface that extends over a unit cell of the plasmonic crystal. The horizontal E field map is detected at the upper border of the top gold layer, while the vertical E field map is detected precisely in the middle of the hole. We will explore the possibilities of precise tuning/ improvement/modification of the geometrical parameters of the structure as we go forward.

Due to the availability of a commercial high power Ti:Sapphire femtosecond laser tunable around 800 nm, we aim to design a photonic crystal with a resonant frequency as close to 800 nm as possible and the conversion efficiency is highly dependent on the peak power, the precise pulse width and the pulse shape of the pump. The source amplitude is defined as follows, to match the average pump laser intensity recorded during the experiments: $Amplitude = \sqrt{\frac{2\,I_{peak}}{\epsilon_0 c}} \sim 10^8\ V/m$ and we have to define the source pulse (~170 fs) in time. The conversion efficiency ($\eta_{TH} = \frac{P_{TH}}{P_{Pump}}$) depends on the intensity (avg. excitation power) and the third order nonlinear susceptibility ($\chi^{(3)}$) value of the gold material. A wavelength dependant $\chi^{(3)}$ database for bulk Au was plugged into the material database of Lumerical.

The polarization field response P of a nonlinear material can be expressed as a power series of E in the following manner.

$$P(t) \simeq \varepsilon_0(\chi^{(1)}E(t) + \chi^{(2)}E(t)E(t) + \chi^{(3)}E(t)E(t)E(t) + \dots)$$

For a centrosymmetric material like metals, even order terms of the susceptibility drop out due to inversion symmetry of the media, yet $\chi^{(3)}$ remains significant. In general the materials anisotropic polarizability must be represented by $\chi^{(n)}$ a n+1 tensor. Crystal symmetry usually allows one to reduce the number of unique components that need to be solved for, and the situation can be further simplified by enforcing linear polarization of the E-field along one of the principle axes.

As a final simplification the electric susceptibility is usually assumed to be dispersionless in the bandwidth of interest. Thus we obtain the following expression for the polarization field:

$$P(t) \simeq \varepsilon_0(\chi^{(1)} + \chi^{(3)})|E(t)|^2E(t)$$

which is plugged into the Maxwell's equations of wave propagation.

Generated TH in reflection is detected by a time monitor placed at the exact same location as the DFT monitor for linear reflectivity, and it records the spectrum of the THG zeroth order (i.e. the FFT of the time signal) at far field.

A two dimensional PhC is periodic along two of its axes and homogeneous along the third. Figure () shows a 2D PhC of hexagonal lattice with lattice parameters as according to the specifications of the fabrication. RI data of SU8 Permanent Epoxy Negative Photoresist was downloaded from the website refractiveindex.info and plugged into Lumerical FDTD as a new material, to have the correct dispersion properties throughout the spectrum of interest.

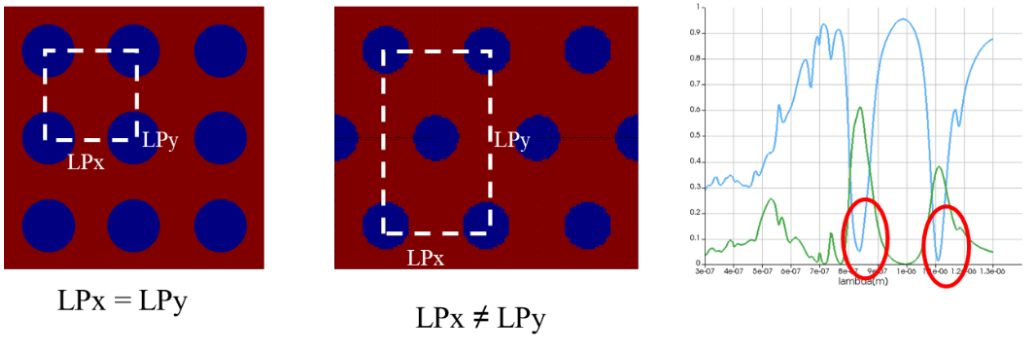

Figure S1: Quasi-3D structure as modelled in FDTD simulations (top view) (a) and (b) shows the square lattice and the hexagonal lattice respectively.

For a square lattice, the unit cell has the same periodicity in both x, y direction, while for a hexagonal lattice the lattice parameters in x, and y direction are different, giving rise to two different resonant wavelengths. The Sharp dips in transmission occur due to light localization at certain wavelengths inside the holes. The spectral position of the resonances are highly dependent on the geometrical parameters of the structure, such as p,d, h1 and h2.

The square lattice has a single resonance, however the hexagonal lattice has two distinct resonances as shown in the Figure() because in the latter case, the lattice parameters are different in x and y direction.

Tunability:

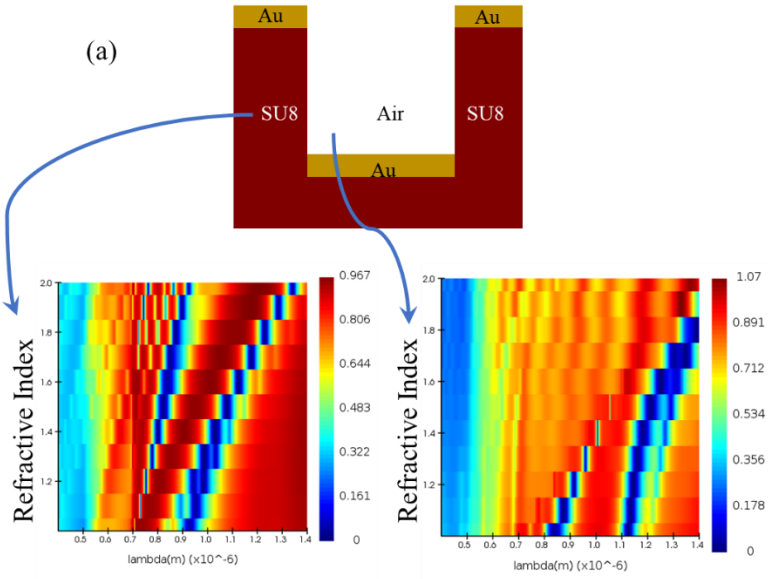

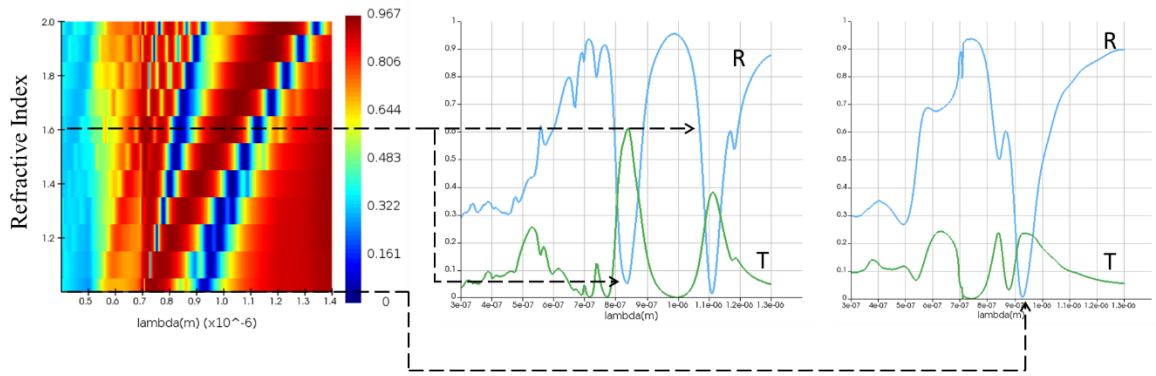

Figure S2: (a) Shift in resonance with change in refractive index of the polymer and refractive index of the material inside the holes (b) Further investigation in to the reflectance map corresponding to the refractive index change of the dielectric reveals two cases: the resonance corresponding to SU8 polymer (Refractive index=1.6) and the purely plasmonic resonance corresponding to the gold periodic structure suspended in Air (Refracrtive index=1)

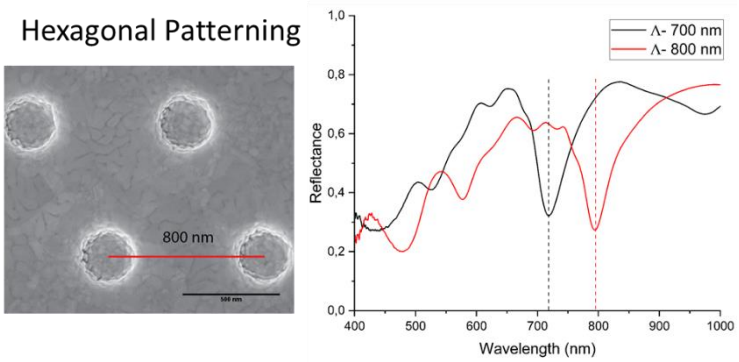

Periodicity p (nm)	**Resonance Position,** λ (nm)
700	718.28
800	790

Figure S3: Shift in resonance with periodicity of the hexagonal patterning

Linear Characterization:

The linear reflectance (0th order) characterization of the photonic crystals was performed in two setups. The 0th order reflectance characteristics of this structure at normal incidence, can resolve the narrowest and the deepest resonance.

For the normal incidence measurements, an FTIR spectrophotometerattached to an optical microscope (Vertex 70 and Hyperion, Bruker)including a linear polarizer was used to obtain the far-field reflectionmeasurements in the 400–850 nm range. Reflected light was collectedthrough a 4× 0.1 NA objective with a spot size of 900 × 900 µm2. Thebackground reflection spectrum was normalized to a silver mirror(96% reflectivity) for both polarizations. The resolution was set to 64cm−1 and 100 scans were recorded with a measurement time greater than 13 seconds. The detector was a Si photodiode, captured through a 4x microscope objective. The spot size was around 400X400 μm^2. A silver mirror reflecting 96% reflectivity was used as a reference.

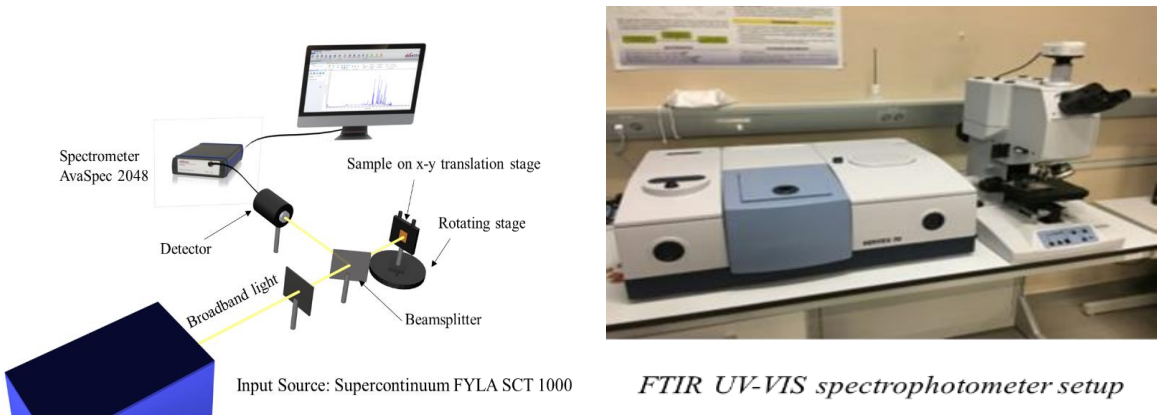

Figure S4: Linear optical characterization setups

The FTIR setup can only measure the reflectance at a normal incidence, so for the angular dispersion measurement, a tabletop varying-angle reflection spectroscopy setup. For this, a supercontinuum laser source (FYLA SCT 1000) was used to illuminate the sample with non-polarized collimated light. The sample was mounted on a rotating platform that is also translational in y-z axis, to make sure the beam hits the patterned part of the sample. The spectrometer used for this section was an AvaSpec 2048 spectrometer with a CMOS detector.

Angular Dispersion:

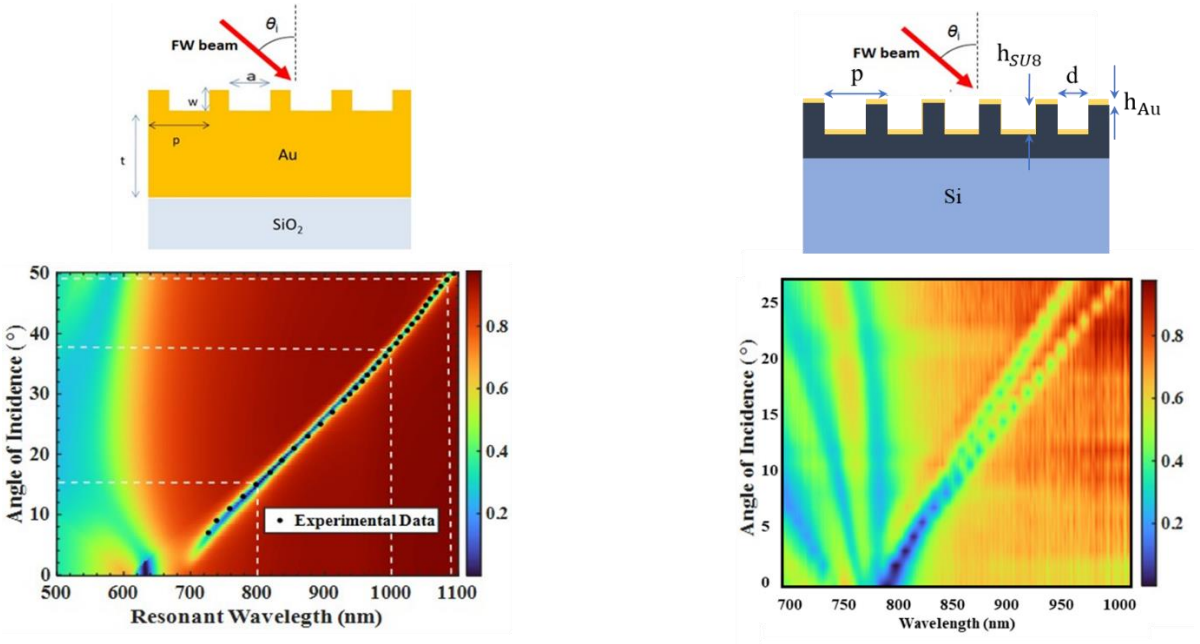

Figure S5: Reflectance map for TM incident polarization broadband sourced as a function of incident angle and wavelength to compare the angular dispersion of a full gold structure and a hybrid structure

Diffraction patterns:

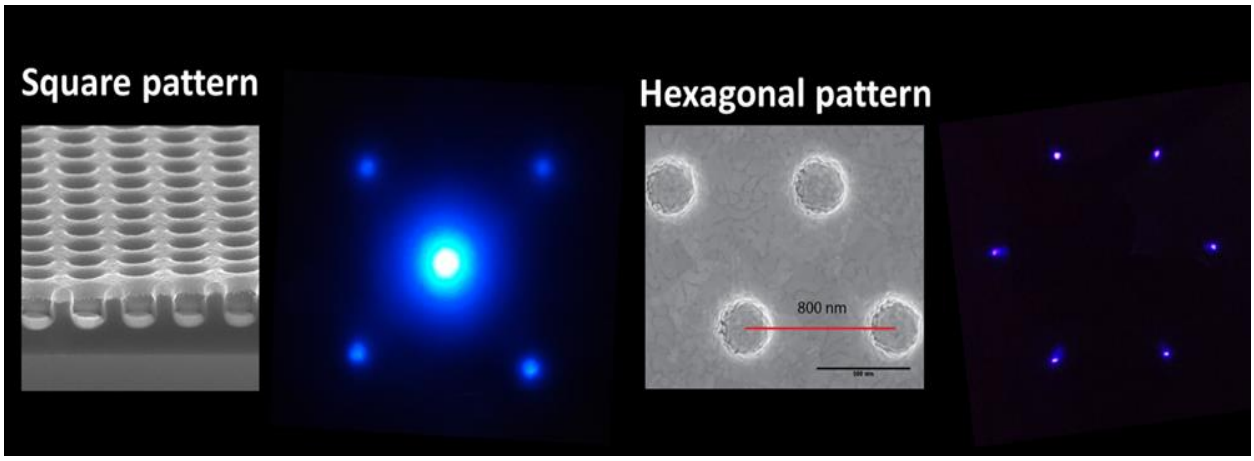

Figure S6: Experimentally verified diffraction pattern of the generated harmonic wavelength, on the left from a square periodicity, on the right from a hexagonal periodicity.